SSRG International Journal of Electrical and Electronics Engineering
ISSN: 2348-8379/ https://doi.org/10.14445/23488379/IJEEE-V11I8P114

Volume 11 Issue 8, 152-167, August 2024

Original Article

Comparison of Hybrid DC-AC Microgrid Energy Management System Using Neural Network and Vector-Decoupled Algorithm Driven by Horse Herd Optimization

Sreenivasula Reddy Pilli[1], Venkata Siva Krishna Rao Gadi[2]

[1,2]*Department of Electrical Engineering, Andhra University, Andhra Pradesh, India.*

[1]*Corresponding Author : sreenivasulareddypilli45@gmail.com*

Received: 06 June 2024 Revised: 09 July 2024 Accepted: 07 August 2024 Published: 31 August 2024

Abstract- *This research paper presents a comparative analysis of Energy Management Systems (EMS) in hybrid DC-AC microgrids, focusing on the application of a neural network vector-decoupled algorithm driven by Horse Herd Optimization (HHO). The objective is to assess the performance and competence of this innovative approach compared to traditional methods in controlling power flow and optimizing energy utilization within microgrid environments. The study begins by outlining the structure and components of a hybrid DC-AC microgrid scheme, emphasizing the incorporation of non-conventional resources, Battery, and the grid. Key components such as converters, inverters, and control mechanisms are discussed to provide a complete empathetic of the scheme. The core focus of this research lies in the comparison between conventional energy management techniques and the proposed neural network vector-decoupled algorithm enhanced by HHO. The neural network algorithm facilitates real-time decision-making and adaptive control, optimizing power flow and enhancing system stability. HHO further enhances the algorithm's efficiency by leveraging the collective intelligence of a simulated horse herd, mimicking their behavior of communication and collaboration for optimization. Simulation studies are done using MATLAB/Simulink to justify the efficacy of the suggested approach. Performance metrics such as system stability, power quality, energy losses, and economic considerations are analyzed and compared against baseline models and existing methodologies. The results demonstrate significant improvements in energy management efficiency, grid stability, and cost-effectiveness with the neural network vector-decoupled algorithm driven by HHO. The paper concludes with insights into the practical implications and future research directions for advancing energy management systems in hybrid DC-AC microgrids.*

Keywords- *Hybrid DC-AC microgrid, Energy Management System (EMS), Neural network, Vector-decoupled algorithm, Horse Herd Optimization.*

1. Introduction

The incorporation of non-conventional resources and energy storage systems into power grids has led to the emergence of microgrids as a promising solution for enhancing energy resilience and sustainability. Among the various types of microgrids, hybrid DC-AC systems play a crucial role in efficiently managing power flow and optimizing energy utilization. These systems combine the benefits of DC and Alternating Current (AC) technologies, offering flexibility and reliability in diverse energy environments. The introduction of a DC-AC microgrid energy management scheme marks a significant advancement in the discipline of energy distribution and management. By integrating non-conventional resources such as PV and wind with ESS like batteries or supercapacitors, these microgrids can function separately or in coincidence with the main grid, ensuring continuous and stable power sources while minimizing environmental impact. This introduction sets the stage for exploring the intricacies of managing energy flow within hybrid DC-AC microgrids, addressing challenges such as grid synchronization, power quality control, and efficient utilization of available resources.

In [1] the reported research on a hybrid power organization employing an optimized ANN and artificial gorilla troops optimizer. The main finding of this study was the successful optimization of the EMS using the proposed algorithm. However, a limitation of this study could be the lack of real-world implementation to validate the effectiveness of the proposed system. In [2] author conducted research on a Hybrid DC-AC microgrid EMS using GWO optimized ANN. The main finding was the improved performance of the EMS

with the optimization technique. A limitation of this study could be the need for further comparative analysis with other optimization algorithms to assess the superiority of the grey wolf optimization approach. In [3] author developed a Real-time EMS for a domestic microgrid. The main finding was the successful implementation of a real-time EMS for a domestic microgrid. A limitation of this study could be the lack of scalability analysis for larger microgrid systems. In [4] author reviewed the main obstacles to power sharing and power organization in a hybrid grid. The main finding was the identification of key challenges that need to be addressed for effective power organization in microgrids. A limitation of this review could be the lack of in-depth analysis of potential solutions to overcome the identified challenges.

In [5] author proposed an EMS for microgrid using an artificial neural network. The main finding was the successful implementation of the ANN for optimizing power organization in microgrids. A limitation of this study could be the need for validation through real-world experiments to approve the efficacy of the suggested method. A power management approach for an ESS in an AC/DC microgrid using modified interlinking converters topology was proposed by the author in [6]. The main finding of this study was the improved competence and permanency of the microgrid scheme. It does not provide a detailed analysis of the economic feasibility of implementing the proposed power management strategy.

In [7] presented an energy management and controller approach for a DC microgrid with an ESS. The study focused on optimizing the energy flow within the microgrid to enhance overall system performance. The study lacks real-world implementation and validation of the recommended EMS and control strategy. In [8] author introduced a bidirectional regulator for microgrid EMS. The study highlighted the importance of bidirectional energy flow control in enhancing the efficiency and stability of microgrids. It does not address the potential challenges and limitations associated with the practical working of bidirectional regulators in microgrid systems. In [9] author took into consideration the dynamic conversion efficacy of reversible AC/DC converters when developing a dynamically coordinated EMS for a microgrid. The study aimed to optimize energy utilization and improve system performance. It does not discuss the impact of varying load conditions on the proposed energy management strategy. In [10] author discussed AC/DC microgrids focusing on Energy organization and power control. The study emphasized the integration of smart technologies to improve the overall working and dependability of the microgrid scheme. The study does not provide a comparative analysis of different power control strategies in AC/DC microgrids.

In [11] author focuses on multi-objective optimization and EMS in a non-conventional energy-reliant microgrid. The main findings include the training of a comprehensive optimization background for efficient power management in such microgrids. The study does not delve into the practical implementation challenges that may arise in real-world scenarios. In [12] author proposes a new microgrid design with a significant ESS. The study highlights the benefits of this architecture in enhancing the overall performance and reliability of the microgrid. It lacks a detailed analysis of the economic feasibility and scalability of the proposed architecture. The author in [13] presents a new dual step EMS approach for a microgrid exploring frequency security constraints. The study emphasizes the importance of ensuring grid stability while optimizing energy management strategies. The research does not address the potential impact of varying load profiles on the proposed energy management scheme. An EMS for a hybrid microgrid based on an SST was suggested by the author in [14].

The study highlights the advantages of using solid-state transformers in improving energy efficiency and grid stability. Limitation: The paper lacks a comparative analysis with traditional transformer-based microgrid systems to showcase the superiority of the proposed strategy. The author in [15] focuses on a hybrid wind/PV/battery energy management scheme for a smart DC microgrid in a smart university setting. The research emphasizes the use of intelligent non-integer control techniques to optimize energy utilization. Limitation: The study does not discuss the potential challenges associated with integrating multiple renewable energy sources into the microgrid system. An AC/DC microgrid design with a complete controller approach for EMS in intelligent buildings was proposed by the author in [16]. The main findings include the development of a control strategy that optimizes energy usage and improves the overall efficiency of the microgrid scheme. Limitations of this consideration may include the lack of real-world implementation and validation of the suggested control approach.

In [17] author presented a microgrid EMS centred on a two-step artificial neural network. The study focused on optimizing energy flow and improving the stability of the microgrid system. A limitation could be the reliance on simulation results without real-world validation [18] presented a hybrid microgrid EMS built on a vector-decoupled approach powered by metaheuristics. In the energy management plan, the research considered electric car charging stations and intermittent renewable energy sources. A limitation may be the complexity of implementing metaheuristic algorithms in real-time applications.

For allocating power and recovering the state of charge of hybrid ESS in multi-DC microgrids, [19] suggested a fuzzy based control technique that relies on frequency decoupling. The study aimed to expand power allocation efficacy and state-of-charge management. A limitation could be the complexity of implementing fuzzy logic control in real-world systems. [20] investigated the EM of a microgrid under

demand response procedures, comparing real-time estimating with pricing. The study focused on optimizing energy consumption based on pricing strategies. A limitation may be the generalizability of the findings to different microgrid configurations and demand response scenarios.

In [21] author spoke about the potential and problems with EMS for AC/DC microgrids. The main findings include the importance of efficient energy management in such systems and the potential advantages of integrating both sources. Limitations of this study could include the focus on challenges and opportunities without providing specific solutions or case studies to support the claims. In [22] author concentrated on employing a PI and ANN based hybrid controller to regulate the energy of a DC microgrid with a hybrid ESS. The main findings highlight the efficacy of the hybrid controller in adjusting energy storage and distribution. A limitation of this study could be the lack of comparison with other types of controllers to determine the superiority of the proposed hybrid controller [23] performed a thorough analysis of the control strategies, optimization methods, and integration issues of AC/DC microgrids. The main findings include the identification of key challenges and the importance of optimization techniques in enhancing the performance of such microgrids. A limitation of this review could be the lack of in-depth analysis of specific optimization techniques or control strategies.

To handle weak power in a hybrid microgrid setting, [24] suggested a unique battery-supported EMS. The main findings emphasize the effectiveness of the battery support in stabilizing power fluctuations. A limitation of this study could be the lack of real-world implementation or validation of the proposed system. In [25] author offered a microgrid's hybrid non-conventional energy scheme for an effective power management and control approach. The main findings include the optimization of power distribution and control approaches for maximizing non-conventional energy utilization. A limitation of this study could be the absence of detailed information on the specific control algorithms used in the proposed strategy.

2. Hybrid DC-AC Microgrids EMS

The block diagram shown in Figure 1 illustrates a hybrid non-conventional energy scheme combining PV and WECS. The solar PV Array captures sunlight, converting it into DC electricity, which is then boosted to match the DC bus voltage via a Boost regulator. The DC bus functions as a conduit for electricity from both the solar array and the battery, serving as a central distribution line within the system.

The Battery acts as an energy reservoir, storing surplus power from the solar and wind systems and providing backup power when renewable sources are inactive. A Bidirectional regulator manages the flow of electricity to and from the battery, converting DC from solar and wind sources to AC for the AC bus or charging the battery from the DC bus. The inverter transforms DC commencing the bus into AC electricity for the AC bus and grid, enabling the system to power AC loads and interact with the utility grid for energy exchange. On the wind side, the Wind Turbine generates AC electricity, which is rectified into DC by a Rectifier for integration into the DC bus. This setup allows for the utilization of wind energy alongside solar energy within the system P&O MPPT procedures optimize the solar array's power output, ensuring efficient energy conversion. In summary, this complex configuration facilitates renewable energy generation, storage, distribution, and grid interaction, offering a comprehensive solution for sustainable power supply to residential or commercial settings.

2.1. Modelling of PV Structure

To model a PV system, we can start by understanding its basic components and the equations governing its behavior. A PV system typically consists of solar panels, a charge governor, an ESS, an inverter for transforming DC to AC and a load consuming the generated electricity. The key equations used in PV system modeling include the current-voltage (I-V) characteristic equation, the power-voltage (P-V) equation, and the equation for power output. The current-voltage characteristic equation of a solar cell is given by,

$$I = I_{ph} - I_0\left(e^{\frac{V+IR_S}{aV_t}} - 1\right) \quad (1)$$

Where I is the current at output, Iph is the photocurrent, I0 is the reverse saturation current, V is the voltage at output, Rs is the resistance linked in series, a is the diode idealist factor, and Vt is the thermal potential.

The power-voltage equation relates the power at output P to the output voltage V and current I as P = IV. For modelling the overall PV system, we consider factors like temperature, solar irradiance, shading, and system losses. The equation for power output can be represented as,

$$P_{out} = P_{max} \times \left(\frac{G}{G_{ref}}\right) \times (1 + \alpha_p \times (T - T_{ref})) \quad (2)$$

Where,
P_{max} is the maximum power output,
G is the irradiance, G_{ref} is the reference irradiance,
α_p is the temperature constant of power,
T is the cell temperature,
T_{ref} is the reference temperature.

These equations, along with models for system losses and efficiency, provide a comprehensive framework for simulating and examining the functioning of a PV scheme under various conditions. Figure 2 shows the flow diagram of P&O MPPT.

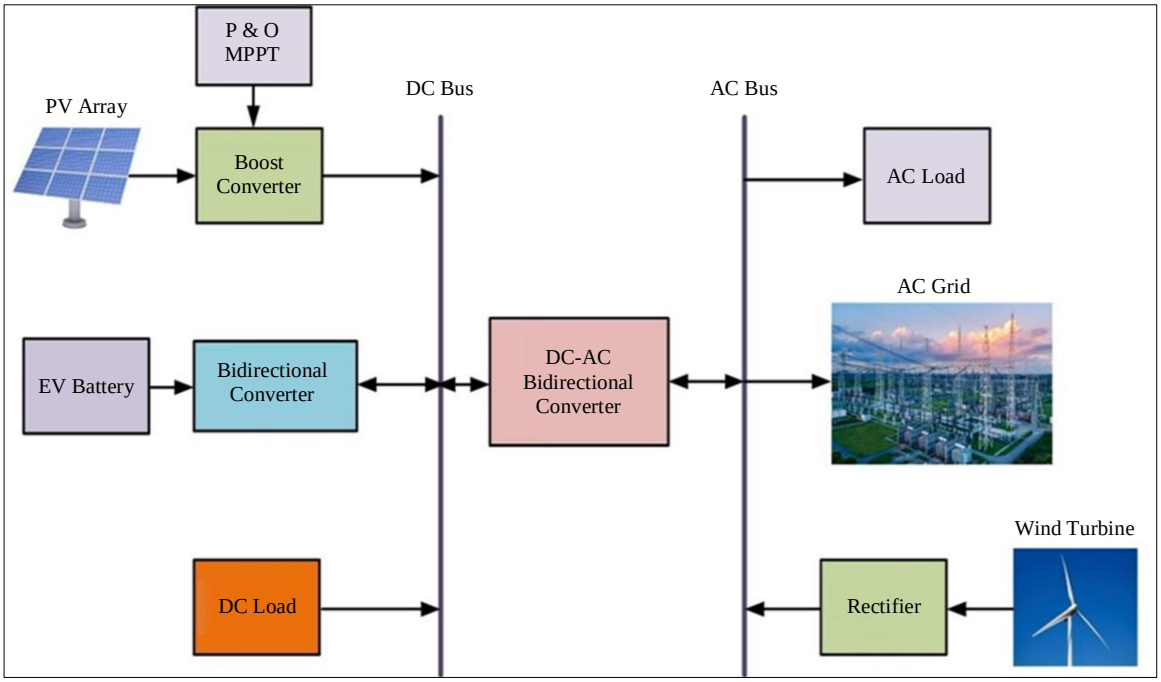

Fig. 1 Overall representation of Hybrid Microgrid system

2.2. P&O MPPT

The provided algorithm outlines the P&O MPPT control technique for a PV scheme. Here is a summary of the steps:

- Set initial values for key variables such as voltage, current, power, perturbation value, and MPPT flag.
- Continuously monitor and measure the PV schemes' voltage and current.
- Calculate the instantaneous power using the measured voltage and current.
- Initially, the MPPT flag is set to 0, indicating the system is not at the MPP.
- Increase the voltage slightly by a perturbation value and measure the new power.
- Make a comparison between the new and prior powers. If the new power is higher, update the MPPT flag and increase the voltage further. If not, decrease the voltage and re-measure the power.
- If the MPPT flag is set, continue perturbing the voltage in the same direction until a decrease in power is observed.
- Once a decrease in power is detected, the system has reached the MPP. Record the voltage and current at this point as optimal operating conditions.
- Adjust the MPPT flag, voltage, and other parameters as needed for ongoing MPPT operation.
- Continuously repeat the steps to track and maintain the PV system at the MPP, accounting for changes in environmental conditions like irradiance or temperature.

This algorithm provides a systematic approach to dynamically adjust the PV system's operating point to maximize power output under varying conditions.

2.3. PV and Its Control Using P&O Method

The PV control system with a boost regulator and P&O MPPT algorithm is designed to optimize the energy outcome of a PV module under varying environmental conditions. At its core, this scheme contains the PV module, which transforms sunlight into DC power, and the MPPT algorithm, such as P&O, which continuously tracks and adjusts the system's operating point to maximize power generation. Key components include the boost converter with its duty cycle control (D), inductor (L), capacitor (C), MOSFET switch (M), Schottky diode (S), and Pulse Width Modulation (PWM) signal.

Figure 3 represents PV and its Control with MPPT. The control operation is intricate yet efficient: the MPPT algorithm monitors the Vpv and Ipv outputs of the PV module, using this data to dynamically modify the duty cycle of the PWM signal. By regulating the switching of the MOSFET and controlling current flow through the inductor and capacitor, the system maintains optimal voltage levels on the DC bus, guaranteeing that the PV scheme operates at its Maximum Power Point (MPP). This meticulous control mechanism ensures that the PV system extracts the highest possible energy from sunlight, contributing to enhanced overall efficiency and performance in renewable energy applications.

2.4. Battery and Its Bidirectional Regulator Control

The explained battery control system, coupled with a bidirectional converter, serves as a crucial component in managing energy flow within renewable energy setups. The bidirectional converter enables versatile functionality by facilitating both the charging and discharging of the battery.

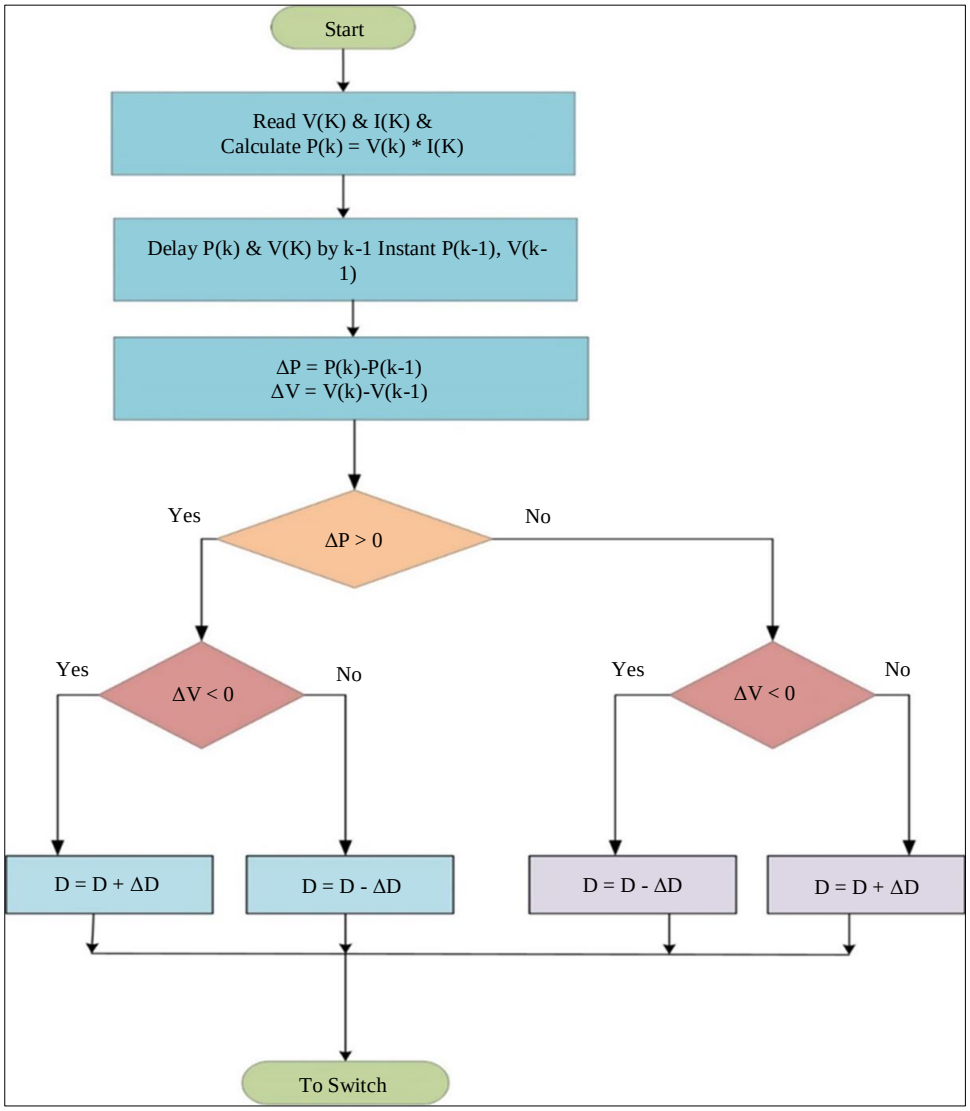

Fig. 2 Flow diagram of P&O MPPT

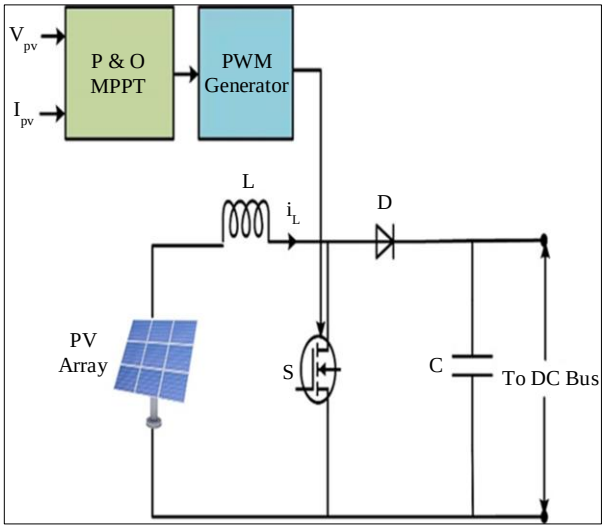

Fig. 3 PV control using P&O MPPT

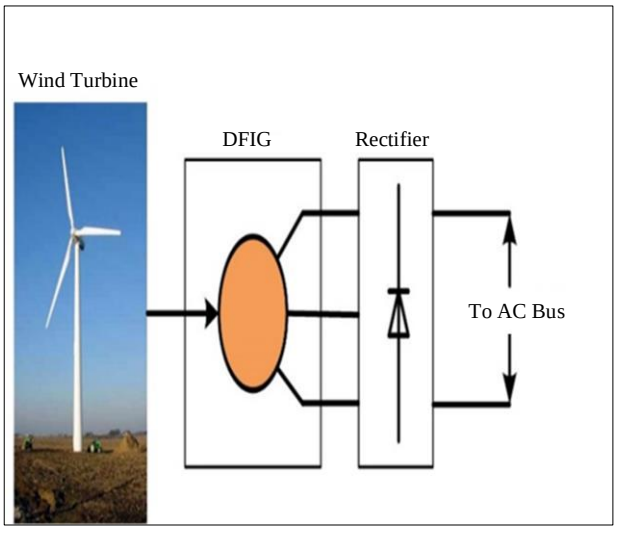

Fig. 4 Wind turbine connected to AC bus

It efficiently converts DC electricity from the DC bus to charge the battery during surplus energy periods, ensuring optimal storage for later use. Conversely, when energy demand exceeds supply, the converter seamlessly switches to discharging mode, supplying power from the battery to the DC bus. This bidirectional capability ensures a balanced energy ecosystem, especially in scenarios where solar or wind energy generation fluctuates.

Central to this system is the PI controller, a sophisticated proportional-integral controller liable for maintaining the voltage at a predefined reference level (Vdcbusref). Through continuous monitoring of the DC bus voltage and comparison with the reference voltage, the PI controller dynamically adjusts the duty cycle of the PWM signal. This fine-tuned modulation of the PWM signal controls the switching of the bidirectional converter switches (S1 and S2), regulating the flow of current between the battery and the DC bus. Consequently, the PI controller ensures that the DC bus voltage remains stable, preventing under or overvoltage conditions and optimizing the overall performance and reliability of the energy storage and distribution system.

2.5. Wind and Its Control

The wind turbine system depicted with a Doubly-Fed Induction Generator (DFIG) and rectifier constitutes an advanced setup for efficient energy conversion from wind power to electrical energy. The DFIG, known for its ability to vary real and reactive power output by adjusting rotor current frequency, significantly enhances power regulation compared to traditional squirrel cage induction generators.

This system's key components include the wind turbine, gearbox for speed adjustment, DFIG with controllable power outputs, converters for AC to DC and vice versa, and a control system ensuring optimal power generation and grid stability. While DFIGs excel in improving power quality, reducing flicker, and capturing energy across a wider range of wind speeds, their complexity and cost are higher compared to simpler induction generators. Utilizing a DFIG in a wind turbine system brings numerous advantages, particularly in enhancing power grid stability and mitigating power output fluctuations caused by wind gusts.

The DFIG's capability to regulate voltage and frequency contributes to improved power quality, while its wider operational range enables increased energy capture across varying wind conditions. However, it is important to note that while DFIGs offer superior performance, they come with higher complexity and cost factors compared to traditional induction generators. These considerations underline the trade-offs involved in selecting the appropriate generator technology for wind energy applications, balancing performance benefits with economic feasibility. The representation of the wind turbine connected to the DC bus is depicted in Figure 4.

2.6. Model and Control of Bidirectional DC-AC Converter

Ensuring stable voltage and frequency levels in hybrid microgrids, especially during disconnection from the main grid's slack bus, poses significant challenges. Synchronous generators within such systems can continue delivering electricity even when disconnected, but excessive demands can lead to frequency shortfalls or voltage collapse.

The primary function of the bidirectional DC-AC regulator in this context is to maintain rigorous control over voltage and frequency under extreme operating conditions. This involves employing double loop controls for both reactive and real power, crucial for intelligently managing the microgrid's DC and AC sides. The control system of the bidirectional DC-AC regulator, as depicted in Figure 5, utilizes a double loop control approach for reactive and real power management. Frequency control hinges on assessing the difference between measured and reference frequencies, adjusting current reference values accordingly.

Similarly, voltage stability is maintained through optimal reactive power flow, with an additional PI controller computing the difference between measured and reference voltages to generate the required reference current. These control parameters, illustrated in Figure 5 as vector-decoupled control parameters, can be optimally tuned using metaheuristic techniques like the horse herd optimization algorithm.

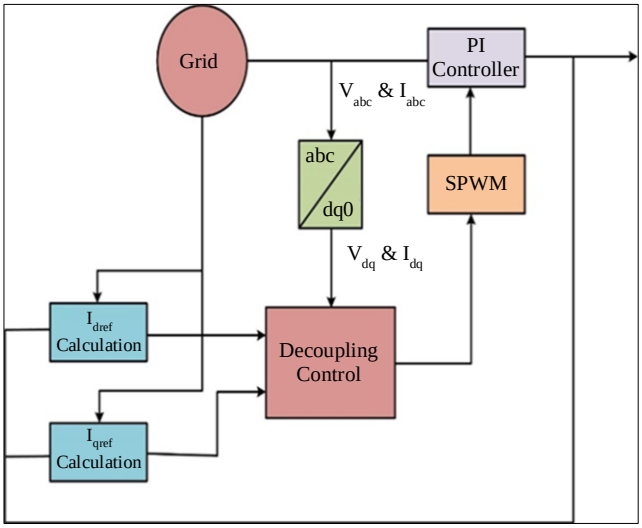

Fig. 5 Representation of DC-AC bidirectional control

3. Control Using ANN and HHO

3.1. ANN Control

Artificial Neural Networks (ANNs) are integral to optimizing energy management in hybrid DC-AC systems, combining Direct Current (DC) and Alternating Current (AC) components. ANNs, mimicking the neural network structure of the human brain, excel in learning intricate patterns and making informed decisions based on input data.

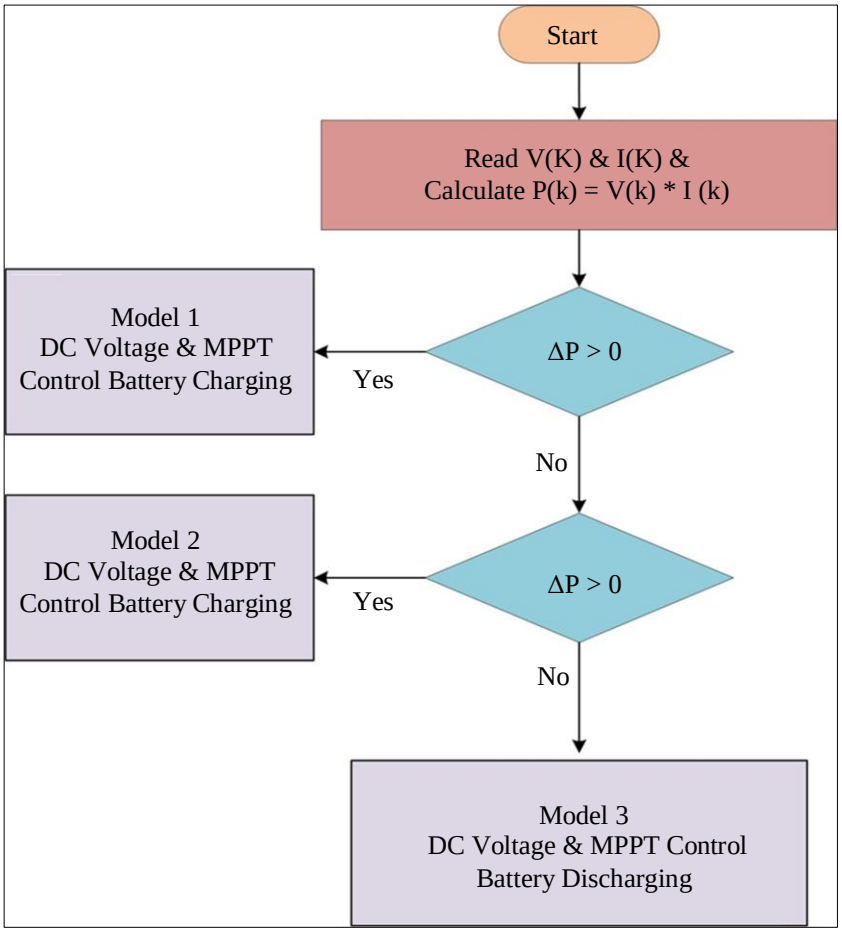

Fig. 6 Energy management using ANN

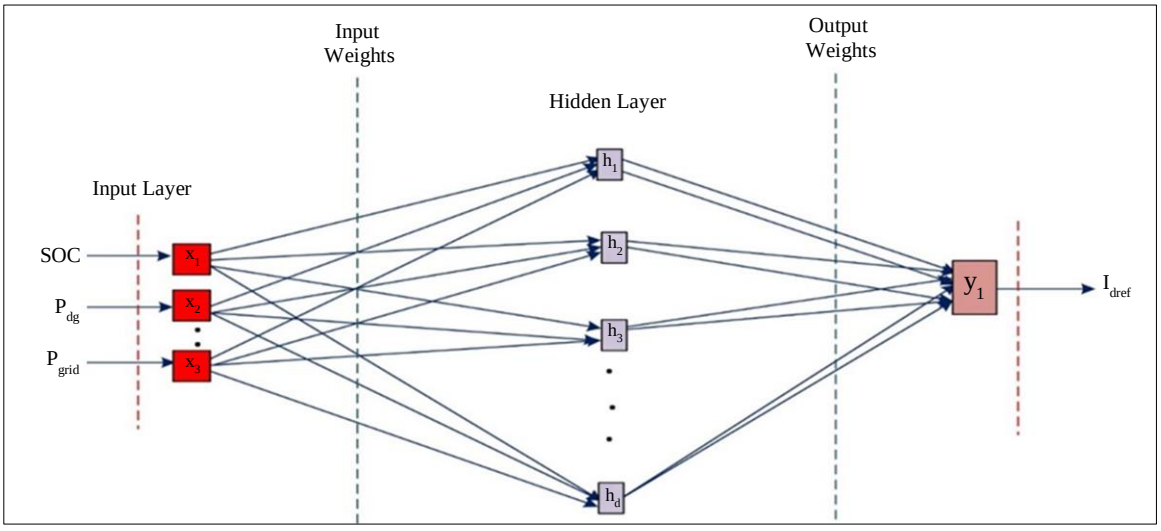

Fig. 7 ANN structure

In the realm of energy management, ANNs address key challenges such as load forecasting by analyzing historical data and external factors to accurately predict energy demand. They also play a crucial role in optimal operation planning, modelling system components and devising strategies for efficient power flow management, thereby minimizing losses and maximizing overall system efficiency. Figure 6 shows the energy management using ANN. Fault detection and diagnostics are significantly contributed by ANNs, leveraging real-time data analysis for detecting anomalies, identifying

component failures, and ensuring proactive maintenance to enhance system reliability.

Their dynamic control capabilities allow for adaptive adjustments of control parameters in response to changing conditions, ensuring peak performance levels and grid stability. ANNs serve as indispensable tools in the pursuit of smarter and greener energy solutions, providing intelligent decision-making capabilities that optimize energy utilization, enhance reliability, and promote sustainability in hybrid DC-AC systems. The layers of ANN are shown in Figure 7.

The hidden layer receives the data from the source layer and forwards it to the resulting layer. Currently, each layer's weighted connections decide its output value. To optimize the output according to the input signal, it is necessary to modify the weight value. We call this procedure "training." Our recommended method uses backpropagation to train the ANN's weights. In this study, data inputs such as battery state of charge, distributed power supply total power generation, and grid power are sent into the ANN's input layer. The direct axis reference current that controls the microgrid to charge or discharge the battery is the ANN's output.

3.2. Horse Herd Optimization Algorithm (HHO)

To operate the HHO, the investigation of how horses behave in their native environments. Horse behavior is frequently characterized by grazing (A), hierarchical (B), social (C), imitation (E), defense mechanisms (D), and roaming (F). This method was, therefore, motivated by the six behaviors of horses at different ages. The equation representing the motion taught to horses at every iteration,

$$Z_i^{iter,AGE} = S_i^{iter,AGE} + Z_i^{(iter-1),AGE}, AGE = \alpha, \beta, \gamma, \delta \quad (3)$$

The position of the ith stallion, AGE representing the stallion's age range, Iter indicating the existing recurrence, and $S_i^{iter,AGE}$ representing the horse's velocity vector are displayed by $Z_i^{iter,AGE}$. Diverse behaviors are exhibited by horses at different ages, with a typical lifespan ranging between 25 and 30 years. Horses aged zero to five years, five to ten years, ten to fifteen years, and over 15 years are denoted by α, β, γ, and δ respectively.

To select stallions' ages, a comprehensive matrix of responses needs to be iteratively considered. By arranging responses in descending order, it becomes feasible to designate 10% of the whole matrix as "horses" for future evaluation. Subsequently, the ensuing 20% of defendants fall into this grouping. 30% of the lasting horses are then categorized as specific types, while the remaining forty percent are classified as other types. Computational simulation has been utilized to model equine behavior and ascertain the horse's velocity.

They feed on various plants in addition to grass and grain since they are herbivores. They spend 16 to 20 hours a day grazing on grass, with very little time for rest. The phrase "continuous eating" refers to eating constantly. Perhaps you have noticed the mares in the pasture with their young. Using an index of gras, the HHO algorithm calculates the amount of grazing area surrounding each horse. Any age of a horse can be observed grazing in the fields. The mathematical representation of grazing is as follows.

$$A_i^{iter,AGE} = {a_i}^{iter,AGE} \times (U + R \times L) \times \left(Z_i^{(iter-1)}\right), \quad AGE = \alpha, \beta, \gamma, \delta \quad (4)$$

$${a_i}^{iter,AGE} = {a_i}^{(iter-1),AGE} \times w_a \quad (5)$$

$A_i^{iter,AGE}$ indicates the horse's propensity for grazing and w_a is the horse's mobility factor. There is less linearity in wg per iteration when this component is taken into account. R is a randomly chosen number within the range of values that this algorithm generates, which goes from 0 to 1. Set U and L to 1.05 and 0.95, respectively, such that Wa remains constant at 1.5 for every age group.

In the wild, horses are not free to act independently. Similar to humans, they adhere to a hierarchical structure and follow a leader. According to this hierarchy, an adult stallion or mare assumes the responsibility of leading groups of wild horses. The coefficient h in the HOA considers the herd's tendency to follow the strongest and most experienced horse. Extensive studies have focused on horses aged between 5 and 15, with their adherence to the hierarchy rule being mathematically expressed.

$$B_i^{iter,AGE} = {b_{iter}}^{iter,AGE} \times \left(Z_*^{(iter-1)} - Z_i^{(iter-1)}\right), \quad AGE = \alpha, \beta, \gamma \quad (6)$$

$${b_i}^{iter,AGE} = {b_i}^{(iter-1),AGE} \times w_b \quad (7)$$

The velocity parameter is highly dependent on the position of the best horse, as demonstrated by$B_i^{iter,AGE}$, and $Z_*^{(iter-1)}$ shows the precise location of the best horse.

Horses require companionship from other animals, sometimes even living in the same home. Predators are now pursuing the stallions, giving them a false feeling of security due to herd life. Plurality facilitates both liberation and survival. Due in large part to their gregarious nature, horses frequently get into conflicts. The horse's distinctiveness is the source of its excitability. Some of the horses get along well with sheep and cattle, and they appear to prefer company over isolation. It appears that the horse is heading towards the center of the group. Young horses (those between the ages of 5 and 15) exhibit high social behavior, which may be explained by the ensuing formula:

$$C_i^{iter,AGE} = c_{iter}{}^{iter,AGE} \times \left(\left(\frac{1}{N}\sum_{k=1}^{N} Z_k^{(iter-1)}\right) - Z_i^{(iter-1)}\right), \quad AGE = \beta, \gamma \tag{8}$$

$$c_i{}^{iter,AGE} = c_i{}^{(iter-1),AGE} \times w_c \tag{9}$$

The ith stallion's social velocity vector is represented by $C_i^{iter,AGE}$, and the ith iteration's orientation towards the herd is denoted by $c_{iter}{}^{iter,AGE}$. With each repetition, $c_{iter}{}^{iter,AGE}$ is reduced by a factor of w_c. The N field encompasses both the total number of horses and the age range of these horses. As part of the factor sensitivity exploration, the c coefficients are computed for β and γ horses.

It is common knowledge that horses pick up on the good and bad habits of their colleagues, including knowing where to find pastures. The current algorithm also takes horse mimicry into account. The innate inclination of a young horse to emulate its elders is expressed in the following equation.

$$E_i^{iter,AGE} = e_{iter}{}^{iter,AGE} \times \left(\left(\frac{1}{pN}\sum_{k=1}^{pN} Z_k^{(iter-1)}\right) - Z_i^{(iter-1)}\right), \quad AGE = \gamma \tag{10}$$

$$e_i{}^{iter,AGE} = e_i{}^{(iter-1),AGE} \times w_e \tag{11}$$

The horse's route concerning the average of the best horses in the region at $Z_i^{(iter-1)}$ locations is represented by the equation $e_i{}^{iter,AGE}$. pN is a representation of the number of horses with the best positions. A ten percent nomination of the horses is needed. The reduction element is represented by w_e in the example above.

The following behavior of horses might be observed because of their mistreatment by predators. They display the fight-or-flight reaction to save themselves. They are born with the need to flee. Moreover, they will buck if they are caught. Horses have an innate need to protect their territory and its supplies against intruders and predators such as wolves.

In the HHO algorithm, a horse's defense strategy is to stay away from other horses who offer false answers. Factor D is crucial to their defense. Horses can choose to run away from danger or to defend themselves. If offered the option, a horse of any age will always select this safety feature. The horse's defense system, which keeps it from being set up inappropriately, is represented by a negative coefficient.

$$D_i^{iter,AGE} = -d_{iter}{}^{iter,AGE} \times \left(\left(\frac{1}{qN}\sum_{k=1}^{qN} Z_k^{(iter-1)}\right) - Z_i^{(iter-1)}\right), \quad AGE = \alpha, \beta, \gamma$$

$$d_i{}^{iter,AGE} = d_i{}^{(iter-1),AGE} \times w_d \tag{12}$$

Where $D_i^{iter,AGE}$ is the outflow vector for the ith stallion from the average of the worst-case placements of the $Z_k^{(iter-1)}$ vector. The overall amount of ponies in the worst-case situation is also mentioned in qN.

Some estimates have the number q at 20% of all horses. The reduction factor is w_d. Horses roam through the countryside for hours on end, from pasture to pasture, in search of food. The majority of horses are kept in stables, while there are few outliers. A horse may suddenly wander off to a different location when it needs to graze. Because of their endless curiosity, horses are constantly searching for new pastures and locations to explore.

The horses' innate curiosity about their surroundings is satiated as they can see one another through the side walls. Simulated as arbitrary motions multiplied by a suitable constant (r). Horses start to roam at a young age, and as they become older, that tendency gradually fades. The flow diagram of HHO is represented in Figure 8.

$$F_i^{iter,AGE} = f_{iter}{}^{iter,AGE} \times \mathcal{P}\left(Z_i^{(iter-1)}\right), AGE = \gamma, \delta \tag{13}$$

$$f_i{}^{iter,AGE} = f_i{}^{(iter-1),AGE} \times w_f \tag{14}$$

For the purpose of local search and avoidance of minimums, a horse's velocity is selected at random. The reduction of the coefficient $F_i^{iter,AGE}$ is shown every cycle by w_f and the arbitrary velocity vector of the ith horse for local search is represented by $f_i{}^{iter,AGE}$. The following equation may be used to represent the specific to age velocity vector of horses after each algorithm iteration.

$$S_i^{iter,\alpha} = A_i^{iter,\alpha} + D_i^{iter,\alpha} \tag{15}$$

$$S_i^{iter,\beta} = A_i^{iter,\beta} + B_i^{iter,\beta} + C_i^{iter,\beta} + D_i^{iter,\beta} \tag{16}$$

$$S_i^{iter,\gamma} = A_i^{iter,\gamma} + B_i^{iter,\gamma} + C_i^{iter,\gamma} + E_i^{iter,\gamma} + D_i^{iter,\gamma} + F_i^{iter,\gamma} \tag{17}$$

$$S_i^{iter,\delta} = A_i^{iter,\delta} + E_i^{iter,\delta} + F_i^{iter,\delta} \tag{18}$$

3.3. Tuning of Decoupled Controlled PI Parameters Using Horse Herd Optimization

There will be no need to become stuck in local optima with this suggested horse herd optimization since it permits concurrent search throughout a population. Six control parameters must be optimized: Kp, Ki value of DC voltage controller, AC voltage controller and current controller. Horse herd optimization to estimate the integral absolute values of RMS voltage and frequency deviation levels in the microgrid's AC section after its dynamic simulation.

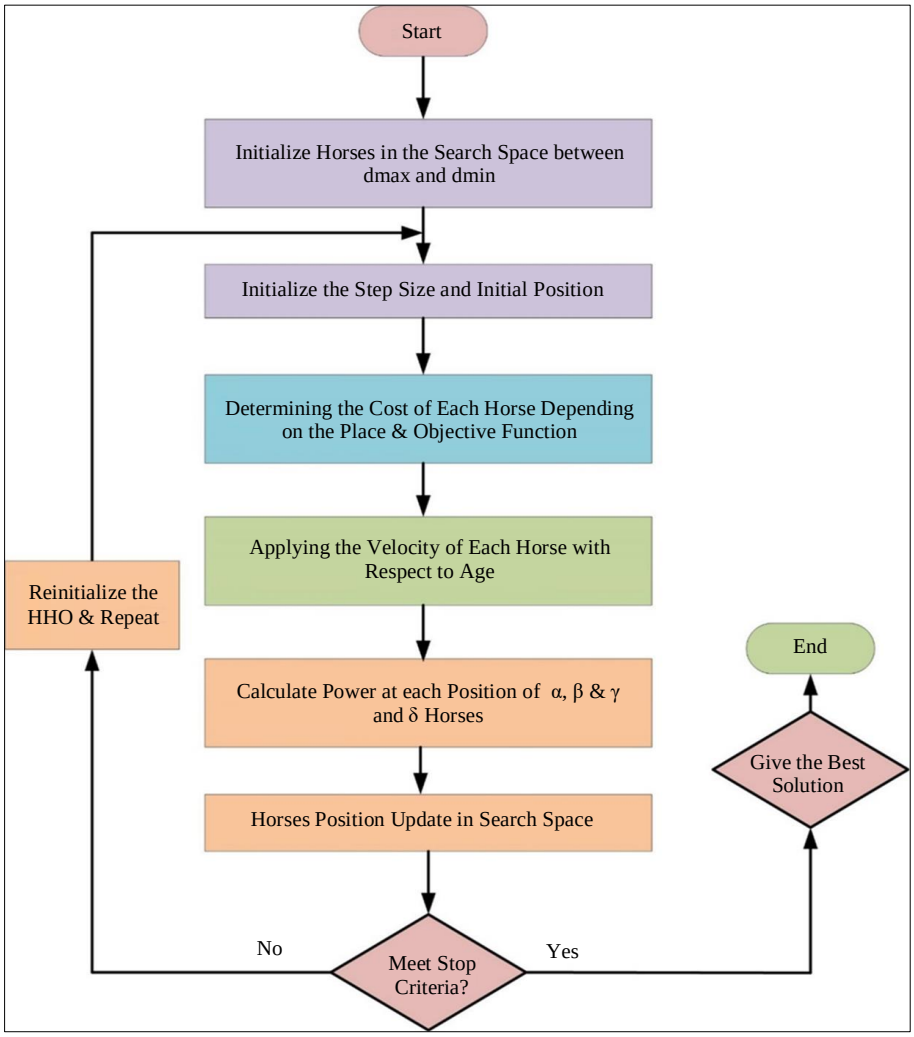

Fig. 8 Flow diagram of HHO

This work uses two fitness functions on the hybrid algorithm to accurately anticipate how the PI controller's gains will self-tune over time. The fitness functions' output is used to regulate the bidirectional converter's energy sharing levels as follows:

$$Fitness = \int \Delta f dt + \int \Delta V dt \quad (19)$$

In order to confirm optimal and safe power distribution among both sides of the hybrid microgrid, we use this search strategy to provide the bidirectional regulator with ideal vector-decoupled control constraints to achieve perfect regulator working and confirm that the system's limits are not exceeded by more than 5% of the base voltage and 3% of the frequency levels.

4. Simulation Results and Discussion

The Simulation of the comparative analysis of ANN & HHO is done in MATLAB/ SIMULINK. Table 1 outlines the parameters used in the simulation of a hybrid microgrid system. The PV section details the photovoltaic array with an MPP voltage Vmp of 29.9 V, current (Imp) of 7.65 A, and maximum power of 228.73 W, consisting of 10 series-linked modules per string and 15 parallel strings. The PV boost converter is specified with an inductance of 0.0105 H, capacitance of 5.2443e-04 F, and a switching frequency of 10 KHz. The wind turbine features a wound rotor type with stator resistance and inductance of 0.023 Ω and 0.18 H, respectively, rotor resistance and inductance of 0.016 Ω and 0.16 H, and a mutual inductance of 2.9 H. The battery system has a nominal voltage of 300 V, a rated capacity of 400 Ah, an initial SOC of 80%, and a response time of 30 seconds. The bidirectional converter includes an inductance of 0.0105 mH and capacitance of 5.2443e-04 µF. The inverter is a 3-level Neutral-Point Clamped (NPC) type. Grid details feature a transformer rating of 34.5/0.4 KV, grid power of 154 MW, voltage of 34.5 KV, and a frequency of 50 Hz. This comprehensive set of parameters facilitates an accurate simulation of the hybrid microgrid's performance under various operating conditions.

Table 1. Parameters used in the simulation

Sl. No.	Specifications	Value
PV Details		
1	Voltage at Maximum Power Point Vmp (V)	29.9
2	Current at Maximum Power Point Imp (A)	7.65
3	Maximum Power (W)	228.73
4	No. of Series-Connected Modules per String	10
5	No of Parallel Strings	15
PV Boost Converter Details		
6	Inductance (H)	0.0105
7	Capacitance (F)	5.2443e-04
8	Switching Frequency (KHz)	10
Wind Details		
9	Type of Rotor	Wound
10	Stator Resistance (Ω) & Inductance (H)	0.023 & 0.18
11	Rotor Resistance (Ω) & Inductance (H)	0.016 & 0.16
12	Mutual Inductance (H)	2.9
Battery Details		
13	Nominal Voltage (V)	300
14	Rated Capacity (Ah)	400
15	Initial State-of-Charge (%)	80
16	Battery Response Time (s)	30
Bidirectional Converter Details		
17	Inductance (mH)	0.0105
18	Capacitance (μF)	5.2443e-04
Inverter Details		
19	Type	3 level NPC
Grid Details		
20	Transformer Rating	34.5/0.4 KV
21	Grid Power (MW) &Voltage (KV)	154 & 34.5
22	Grid Frequency (HZ)	50

The variation in irradiance of the PV array, as shown in Figure 9, demonstrates how the sunlight intensity fluctuates over time. Initially, the irradiance starts at 1000 W/m² and gradually decreases from 1 second until it reaches 0 W/m² at 10 seconds. This period of decline represents a scenario where sunlight is diminishing, such as during sunset or cloud cover. After reaching 0 W/m², the irradiance begins to increase again, simulating conditions where sunlight starts to return, possibly due to sunrise or the dissipation of clouds. Figure 10 presents a similarity of PV power output linking the HHO and ANN control methods under these varying irradiance conditions. At the peak irradiance of 1000 W/m², the PV power output using HHO is 34.31 kW, whereas the output using ANN is slightly lower at 33.62 kW. This indicates that the HHO control method is more effective at harnessing the available solar energy, resulting in higher power generation compared to the ANN method.

This comparative analysis highlights the robustness and efficiency of the HHO algorithm in optimizing PV power output, even under fluctuating irradiance conditions. The superior performance of HHO is evident in its ability to maintain higher power levels, making it a more reliable and effective control strategy for managing PV systems in dynamic environments.

The battery power comparison of HHO & ANN during varying PV power is showcased in Figure 11. It clearly indicates that according to the availability of the input power, the charging and discharging condition of the battery will vary. The comparison of grid power using the HHO and ANN techniques is illustrated in Figure 12. During the time interval from 0 to 10 seconds, the grid receives power from various sources, which are represented as negative values, indicating the direction of power flow towards the grid.

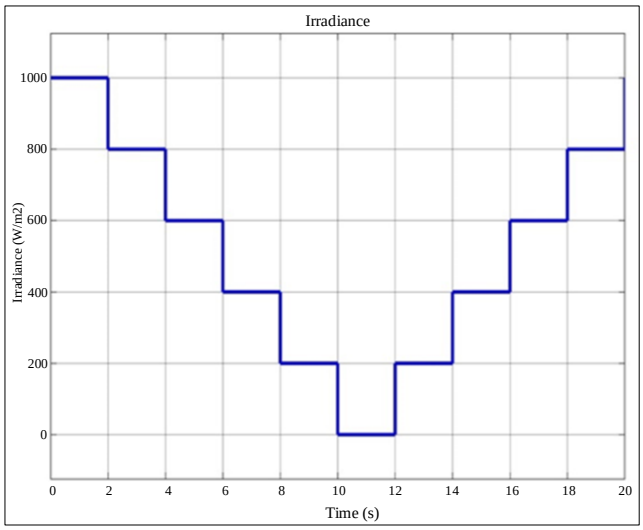

Fig. 9 Variation in Irradiance of the PV array

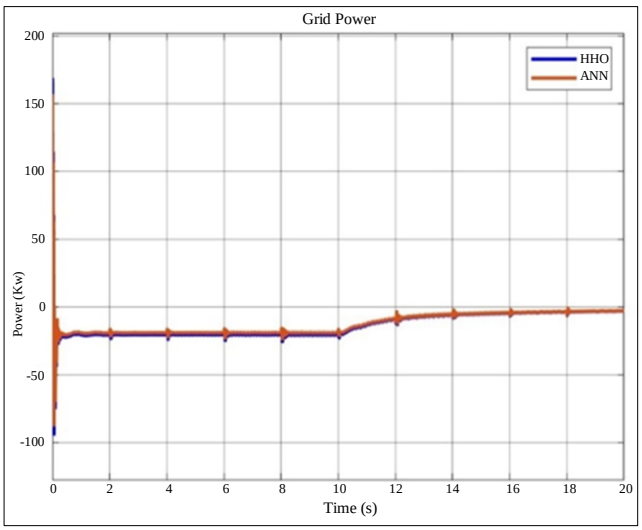

Fig. 12 Comparison of the Grid power with HHO & ANN

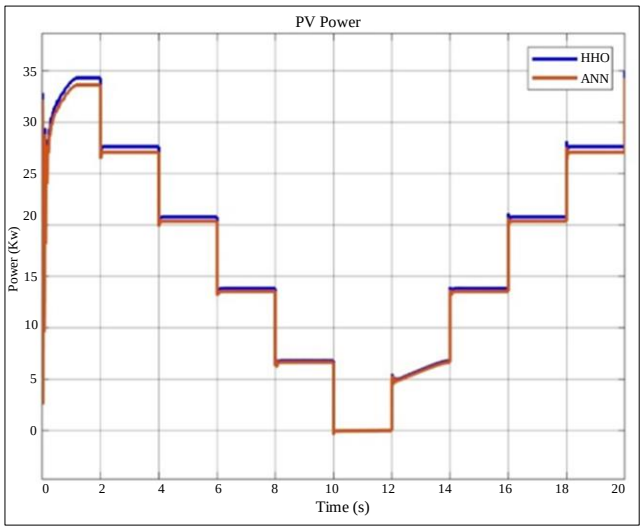

Fig. 10 Comparison of the PV power with HHO & ANN

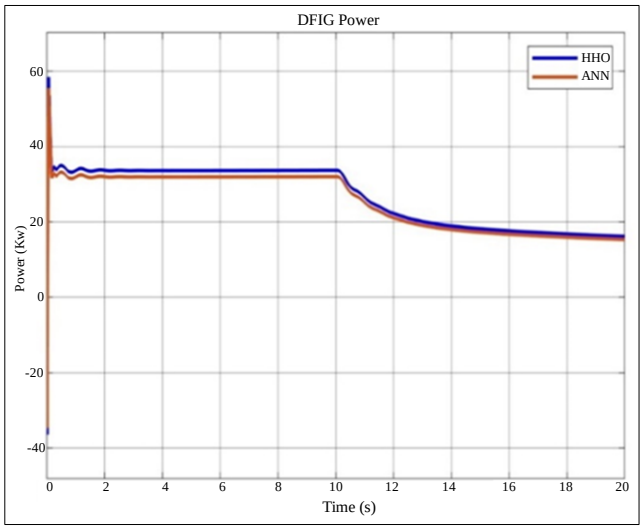

Fig. 13 Comparison of the DFIG power with HHO & ANN

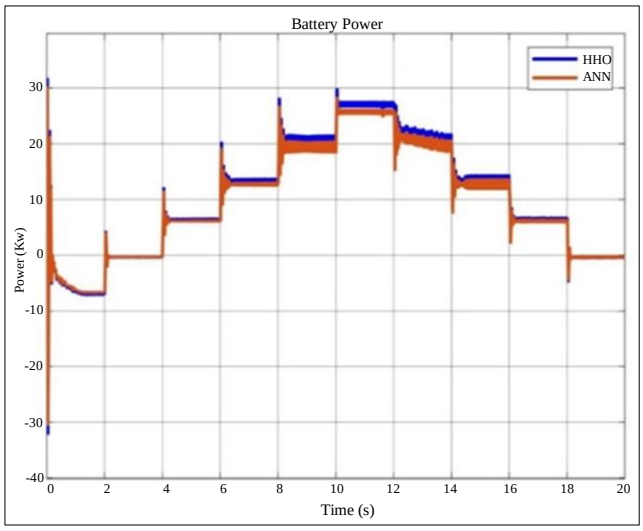

Fig. 11 Comparison of the battery power with HHO & ANN

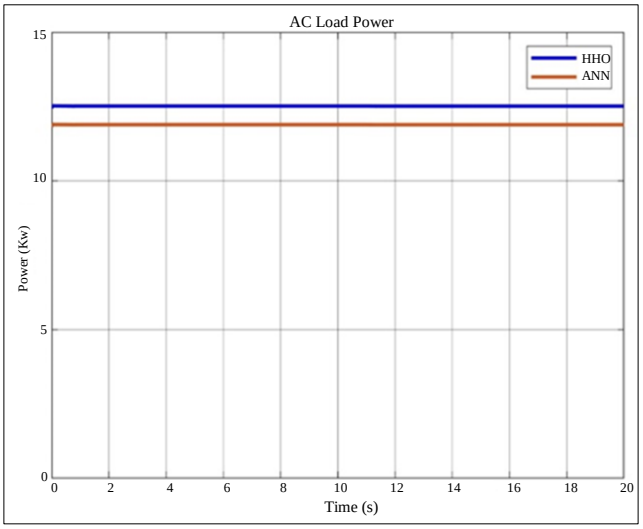

Fig. 14 Comparison of the AC load power with HHO & ANN

Figure 13 presents the power output from the DFIG connected to the wind turbine. Here, the power outputs achieved using HHO and ANN are 33.75 kW and 32.06 kW, respectively. This demonstrates the slight variation in the performance of the two methods in harnessing wind energy. In Figure 14, the comparison of AC load power is shown. The AC load power obtained using ANN is 11.89 kW, whereas for HHO, it is 12.52 kW. This indicates that the HHO method provides a marginally higher AC load power compared to ANN.

Figure 15 provides a comparison of the duty cycles for both optimization methods. The duty cycle comparison is crucial as it reflects the control mechanism's efficiency in regulating the power converters within the microgrid system. By analyzing these figures, one can observe the operational differences and performance efficiencies between HHO and ANN in managing and optimizing the power distribution in a hybrid microgrid system. The detailed comparison highlights the strengths and potential advantages of using HHO over ANN in specific scenarios, such as maximizing power output from renewable sources and effectively managing AC load demands.

The Comparison of the DC link voltage is represented in Figure 16. Here the HHO maintains a constant DC voltage, when compared with ANN. The representation of the DC link current is given in Figure 17. The DC load power comparison using HHO and ANN control methods is illustrated in Figure 18. The results indicate that the DC load power achieved with ANN control is 9.49 kW, while with HHO control, it is 9.99 kW. This indicates that HHO control delivers slightly higher DC load power, showcasing its efficiency in managing the power distribution within the microgrid.

Figure 19 depicts the SOC of the battery, which varies according to the charging and discharging cycles. The SOC is a critical parameter that reflects the battery's available capacity and overall health. As the battery charges, the SOC increases, and as it discharges, the SOC decreases. The fluctuation of SOC in the figure highlights the dynamic nature of the ESS under different control methods. Figure 20 presents the battery current, which further elucidates the battery's charging and discharging behavior. The battery current graph helps in understanding the rate at which the battery is being charged or discharged over time. Variations in the current indicate how effectively the control algorithms manage the power flow to and from the battery, ensuring the ideal performance and longevity of the battery storage system.

Table 2 provides a comparative analysis of power outputs using ANN and HHO techniques under an irradiance condition of 1000 W/m² for the Photovoltaic (PV) system. The PV power generated is slightly higher with HHO at 34.31 kW compared to 33.62 kW with ANN, indicating a more efficient utilization of solar energy by the HHO method.

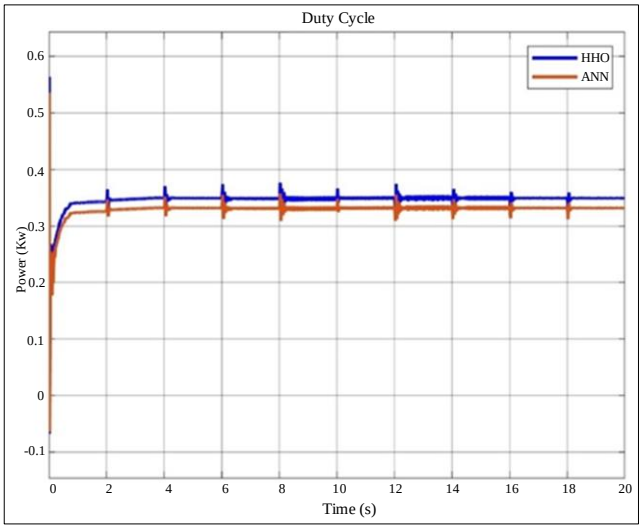

Fig. 15 Comparison of the Duty cycle with HHO & ANN

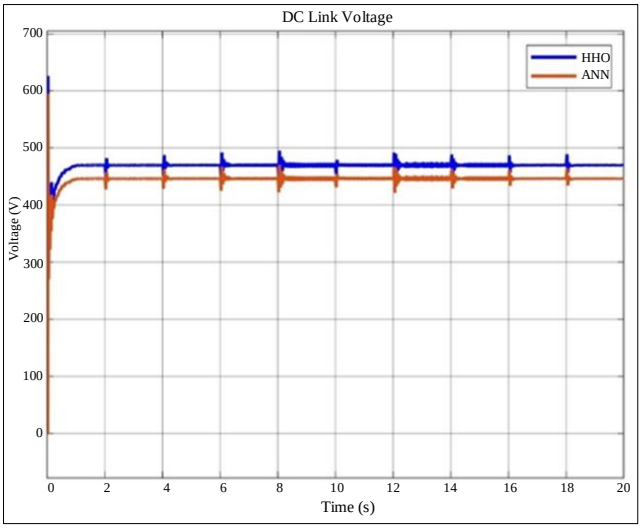

Fig. 16 Comparison of the DC link voltage with HHO & ANN

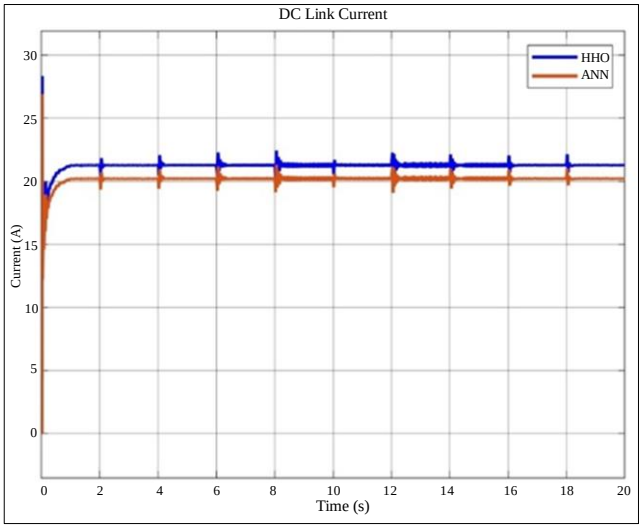

Fig. 17 Comparison of the DC link current with HHO & ANN

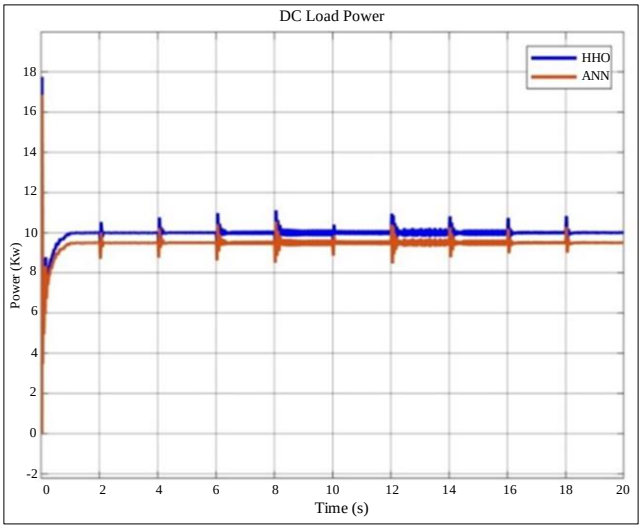

Fig.18 Comparison of the DC load power with HHO & ANN

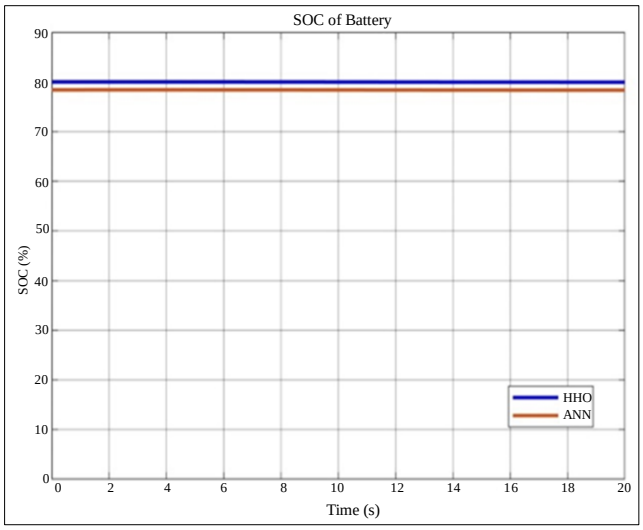

Fig. 19 Comparison of the SOC of battery with HHO & ANN

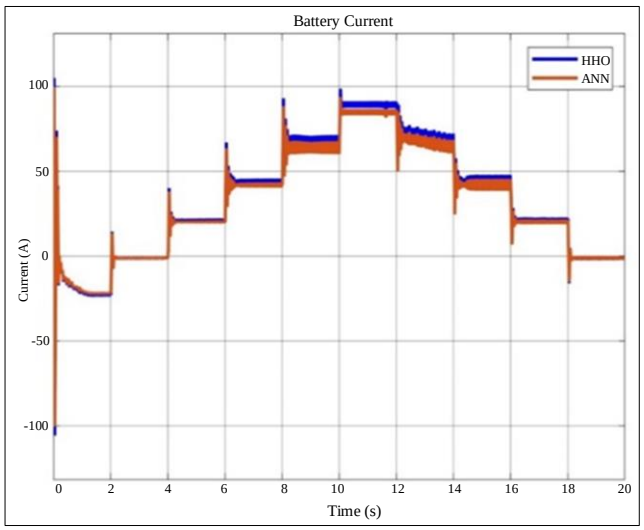

Fig. 20 Comparison of the battery current with HHO & ANN

Table 2. Comparison of powers with ANN & HHO

Parameters	ANN	HHO
PV Power (KW)	33.62	34.31
Grid Power (KW)	19.25	20.70
Battery Power (KW)	-6.696	-7.048
DFIG Power (KW)	32.06	33.75
AC Load Power (KW)	11.89	12.52
DC Load Power (KW)	9.49	9.99

For grid power, the table shows -19.25 kW for ANN and 20.70 kW for HHO. The negative sign for ANN indicates that the grid is receiving power from the sources, whereas with HHO, the grid is supplying power to the system, showcasing a significant difference in power flow management between the two techniques.

The battery power values are -6.696 kW for ANN and -7.048 kW for HHO, with the negative sign indicating that the battery is in charging mode in both cases. The Doubly-Fed Induction Generator (DFIG) power from the wind turbine shows outputs of 32.06 kW for ANN and 33.75 kW for HHO, again demonstrating the higher efficiency of HHO in harnessing wind energy.

Additionally, the AC load power is 11.89 kW for ANN and 12.52 kW for HHO, while the DC load power is 9.49 kW for ANN and 9.99 kW for HHO. These comparisons highlight that HHO generally results in higher power outputs for both AC and DC loads, indicating its potential for better overall performance in managing and optimizing the hybrid microgrid system.

Using the proposed system, the PV power and Grid power have been improved compared to the existing system and is shown in Table 3.

Table 3. Power comparison of proposed ANN & HHO

Technique/ Parameter	PV Power (KW)	Grid Power (KW)
LMNN [1]	27.4	18.31
GANN [1]	27.5	18.56
PSONN [1]	27.2	18.31
Cuckoo-NN [1]	27.1	18.3
GTONN [1]	26.9	18.4
ANN	33.62	19.25
Proposed HHO	**34.31**	**20.70**

5. Conclusion

This study has compared the performance of a Hybrid DC-AC microgrid energy management system utilizing an ANN and a Vector-Decoupled Algorithm driven by HHO. The comparison was based on various power output parameters under a consistent PV irradiance of 1000 W/m². The numerical data clearly indicates that HHO outperforms ANN across multiple metrics. The PV power generated using HHO was 34.31 kW, slightly higher than the 33.62 kW generated with ANN. This shows a more efficient utilization of solar energy by the HHO-driven system.

Furthermore, grid power management differed significantly, with ANN recording -19.25 kW, indicating that the grid was receiving power, while HHO recorded 20.70 kW, suggesting that the grid was supplying power. This highlights the superior power flow management capability of the HHO method. Battery charging power also favoured HHO, with -7.048 kW compared to -6.696 kW for ANN, indicating more efficient energy storage. The DFIG power from the wind turbine was 33.75 kW for HHO, surpassing the 32.06 kW achieved by ANN.

Additionally, HHO provided higher AC load power (12.52 kW) and DC load power (9.99 kW) compared to ANN's 11.89 kW and 9.49 kW, respectively. In summary, the Vector-Decoupled Algorithm driven by Horse Herd Optimization demonstrated superior performance in energy management for the hybrid DC-AC microgrid system compared to the Neural Network approach. The numerical results underscore HHO's potential for enhancing the efficiency, reliability, and overall performance of microgrid energy systems.

References

[1] Sathesh Murugan, Mohana Jaishankar, and Kamaraj Premkumar, "Hybrid DC-AC Microgrid Energy Management System Using an Artificial Gorilla Troops Optimizer Optimized Neural Network," *Energies*, vol. 15, no. 21, pp. 1-19, 2022. [CrossRef] [Google Scholar] [Publisher Link]

[2] S. Sahaya Elsi, F. Michael Raj, and S. Prince Mary, "Hybrid DC-AC Microgrid Energy Management System Using Grey Wolf Optimized Neural Network," *Journal of Intelligent & Fuzzy Systems*, vol. 44, no. 4, pp. 6885-6899, 2023. [CrossRef] [Google Scholar] [Publisher Link]

[3] Enrique Rodriguez-Diaz et al., "Real-Time Energy Management System for a hybrid AC/DC Residential Microgrid," *2017 IEEE Second International Conference on DC Microgrids (ICDCM)*, Nuremburg, Germany, pp. 256-261, 2017. [CrossRef] [Google Scholar] [Publisher Link]

[4] Sohail Sarwar et al., "Major Challenges Towards Energy Management and Power Sharing in a Hybrid AC/DC Microgrid: A Review," *Energies*, vol. 15, no. 23, pp. 1-30, 2022. [CrossRef] [Google Scholar] [Publisher Link]

[5] Kyung-Min Kang et al., "Energy Management Method of Hybrid AC/DC Microgrid Using Artificial Neural Network," *Electronics*, vol. 10, no. 16, pp. 1-29, 2021. [CrossRef] [Google Scholar] [Publisher Link]

[6] Joao Pedro Carvalho Silveira et al., "Power Management of Energy Storage System with Modified Interlinking Converters Topology in Hybrid AC/DC Microgrid," *International Journal of Electrical Power & Energy Systems*, vol. 130, 2021. [CrossRef] [Google Scholar] [Publisher Link]

[7] Hassan Abouobaida et al., "Energy Management and Control Strategy of DC Microgrid Based Hybrid Storage System," *Simulation Modelling Practice and Theory*, vol. 124, 2023. [CrossRef] [Google Scholar] [Publisher Link]

[8] R. Rajasekaran, and P. Usha Rani, "Bidirectional DC-DC Converter for Microgrid in Energy Management System," *International Journal of Electronics*, vol. 108, no. 2, pp. 322-343, 2021. [CrossRef] [Google Scholar] [Publisher Link]

[9] Bin Wei et al., "Temporally Coordinated Energy Management for AC/DC Hybrid Microgrid Considering Dynamic Conversion Efficiency of Bidirectional AC/DC Converter," *IEEE Access*, vol. 8, pp. 70878-70889, 2020. [CrossRef] [Google Scholar] [Publisher Link]

[10] Yunwei Ryan Li, Farzam Nejabatkhah, and Hao Tian, *Smart Hybrid AC/DC Microgrids: Power Management, Energy Management, and Power Quality Control*, John Wiley & Sons, 2022. [CrossRef] [Google Scholar] [Publisher Link]

[11] Indragandhi V. et al., "Multi-Objective Optimization and Energy Management in Renewable Based AC/DC Microgrid," *Computers & Electrical Engineering*, vol. 70, pp. 179-198, 2018. [CrossRef] [Google Scholar] [Publisher Link]

[12] Moudud Ahmed et al., "A Novel Hybrid AC/DC Microgrid Architecture with a Central Energy Storage System," *IEEE Transactions on Power Delivery*, vol. 37, no. 3, pp. 2060-2070, 2022. [CrossRef] [Google Scholar] [Publisher Link]

[13] Zhongwen Li et al., "A Novel Two-Stage Energy Management of Hybrid AC/DC Microgrid Considering Frequency Security Constraints," *International Journal of Electrical Power & Energy Systems*, vol. 146, 2023. [CrossRef] [Google Scholar] [Publisher Link]

[14] Zhengwei Qu et al., "Energy Management Strategy of AC/DC Hybrid Microgrid Based on Solid-State Transformer," *IEEE Access*, vol. 10, pp. 20633-20642, 2022. [CrossRef] [Google Scholar] [Publisher Link]

[15] Ahmad Aziz Al Alahmadi et al., "Hybrid Wind/PV/Battery Energy Management-Based Intelligent Non-Integer Control for Smart DC-Microgrid of Smart University," *IEEE Access*, vol. 9, pp. 98948-98961, 2021. [CrossRef] [Google Scholar] [Publisher Link]

[16] Yahui Wang et al., "Hybrid AC/DC Microgrid Architecture with Comprehensive Control Strategy for Energy Management of Smart Building," *International Journal of Electrical Power & Energy Systems*, vol. 101, pp. 151-161, 2018. [CrossRef] [Google Scholar] [Publisher Link]

[17] Tae-Gyu Kim et al., "Hybrid AC/DC Microgrid Energy Management Strategy Based on Two-Step ANN," *Energies*, vol. 16, no. 4, pp. 1-23, 2023. [CrossRef] [Google Scholar] [Publisher Link]

[18] Tawfiq M. Aljohani, Ahmed F. Ebrahim, and Osama Mohammed, "Hybrid Microgrid Energy Management and Control Based on Metaheuristic-Driven Vector-Decoupled Algorithm Considering Intermittent Renewable Sources and Electric Vehicles Charging Lot," *Energies*, vol. 13, no. 13, pp. 1-19, 2020. [CrossRef] [Google Scholar] [Publisher Link]

[19] Mohamed Amine Hartani et al., "Proposed Frequency Decoupling-Based Fuzzy Logic Control for Power Allocation and State-of-Charge Recovery of Hybrid Energy Storage Systems Adopting Multi-Level Energy Management for Multi-DC-Microgrids," *Energy*, vol. *278*, 2023. [CrossRef] [Google Scholar] [Publisher Link]

[20] Ramin Nourollahi, Kazem Zare, and Sayyad Nojavan, "Energy Management of Hybrid AC-DC Microgrid under Demand Response Programs: Real-Time Pricing versus Time-of-Use Pricing," *Demand Response Application in Smart Grids*, pp. 75-93, 2019. [CrossRef] [Google Scholar] [Publisher Link]

[21] Moein Manbachi, "Energy Management Systems for Hybrid AC/DC Microgrids: Challenges and Opportunities," *Operation of Distributed Energy Resources in Smart Distribution Networks*, pp. 303-348, 2018. [CrossRef] [Google Scholar] [Publisher Link]

[22] Amit Kumar Rajput, and J.S. Lather, "Energy Management of a DC Microgrid with Hybrid Energy Storage System Using PI and ANN Based Hybrid Controller," *International Journal of Ambient Energy*, vol. 44, no. 1, pp. 703-718, 2022. [CrossRef] [Google Scholar] [Publisher Link]

[23] Omar Azeem et al., "A Comprehensive Review on Integration Challenges, Optimization Techniques and Control Strategies of Hybrid AC/DC Microgrid," *Applied Sciences*, vol. 11, no. 14, pp. 1-32, 2021. [CrossRef] [Google Scholar] [Publisher Link]

[24] Sivasankar Gangatharan et al., "A Novel Battery Supported Energy Management System for the Effective Handling of Feeble Power in Hybrid Microgrid Environment," *IEEE Access*, vol. 8, pp. 217391-217415, 2020. [CrossRef] [Google Scholar] [Publisher Link]

[25] J. Vinothkumar, and R. Thamizhselvan, "Efficient Power Management and Control Strategy of Hybrid Renewable Energy System in Microgrid," *International Journal on Applied Physics and Engineering*, vol. 2, pp. 106-127, 2023. [CrossRef] [Google Scholar] [Publisher Link]